

This work was written as part of one of the author's official duties as an Employee of the United States Government and is therefore a work of the United States Government. In accordance with 17 U.S.C. 105, no copyright protection is available for such works under U.S. Law.

Public Domain Mark 1.0

<https://creativecommons.org/publicdomain/mark/1.0/>

Access to this work was provided by the University of Maryland, Baltimore County (UMBC) ScholarWorks@UMBC digital repository on the Maryland Shared Open Access (MD-SOAR) platform.

**Please provide feedback**

Please support the ScholarWorks@UMBC repository by emailing [scholarworks-group@umbc.edu](mailto:scholarworks-group@umbc.edu) and telling us what having access to this work means to you and why it's important to you. Thank you.

# Status of Xtend telescope onboard X-Ray Imaging and Spectroscopy Mission (XRISM)

Koji Mori<sup>a</sup>, Hiroshi Tomida<sup>b</sup>, Hiroshi Nakajima<sup>c</sup>, Takashi Okajima<sup>d</sup>, Hirofumi Noda<sup>e</sup>, Hiroyuki Uchida<sup>f</sup>, Hiromasa Suzuki<sup>b</sup>, Shogo Benjamin Kobayashi<sup>g</sup>, Tomokage Yoneyama<sup>h</sup>, Kouichi Hagino<sup>i</sup>, Kumiko Nobukawa<sup>j</sup>, Takaaki Tanaka<sup>k</sup>, Hiroshi Murakami<sup>l</sup>, Hideki Uchiyama<sup>m</sup>, Masayoshi Nobukawa<sup>n</sup>, Hironori Matsumoto<sup>o,p</sup>, Takeshi Tsuru<sup>f</sup>, Makoto Yamauchi<sup>a</sup>, Isamu Hatsukade<sup>a</sup>, Hirokazu Odaka<sup>o,p</sup>, Takayoshi Kohmura<sup>q</sup>, Kazutaka Yamaoka<sup>r</sup>, Manabu Ishida<sup>b</sup>, Yoshitomo Maeda<sup>b</sup>, Takayuki Hayashi<sup>f,s</sup>, Keisuke Tamura<sup>f,s</sup>, Rozenn Boissay-Malaquin<sup>f,s</sup>, Toshiki Sato<sup>t</sup>, Tessei Yoshida<sup>u</sup>, Yoshiaki Kanemaru<sup>b</sup>, Junko Hiraga<sup>v</sup>, Tadayasu Dotani<sup>b,w</sup>, Masanobu Ozaki<sup>x</sup>, Hiroshi Tsunemi<sup>o</sup>, Shun Inoue<sup>f</sup>, Ryuishi Azuma<sup>m</sup>, Yuma Aoki<sup>k</sup>, Yoh Asahina<sup>c</sup>, Shotaro Nakamura<sup>c</sup>, Takamitsu Kamei<sup>c</sup>, Masahiro Fukuda<sup>c</sup>, Kazunori Asakura<sup>o</sup>, Marina Yoshimoto<sup>o</sup>, Yuichi Ode<sup>o</sup>, Tomohiro Hakamata<sup>o</sup>, Mio Aoyagi<sup>o</sup>, Kohei shima<sup>o</sup>, Yuma Aoki<sup>j</sup>, Yamato Ito<sup>j</sup>, Daiki Aoki<sup>q</sup>, Kaito Fujisawa<sup>q</sup>, Yasuyuki Shimizu<sup>q</sup>, Mayu Higuchi<sup>q</sup>, Keitaro Miyazaki<sup>a</sup>, Kohei Kusunoki<sup>a</sup>, Yoshinori Otsuka<sup>a</sup>, Haruhiko Yokosu<sup>a</sup>, Wakana Yonemaru<sup>a</sup>, Kazuhiro Ichikawa<sup>a</sup>, Hanako Nakano<sup>a</sup>, Reo takemoto<sup>a</sup>, Tsukasa Matsushima<sup>a</sup>, and Kiyoshi Hayashida<sup>o</sup>

<sup>a</sup>Faculty of Engineering, University of Miyazaki, 1-1 Gakuen Kibanadai Nishi, Miyazaki, Miyazaki 889-2192, Japan

<sup>b</sup>Japan Aerospace Exploration Agency, Institute of Space and Astronautical Science, 3-1-1 Yoshino-dai, Chuo-ku, Sagamihara, Kanagawa 252-5210, Japan

<sup>c</sup>College of Science and Engineering, Kanto Gakuinn University, Kanazawa-ku, Yokohama, Kanagawa 236-8501, Japan

<sup>d</sup>NASA's Goddard Space Flight Center, Greenbelt, MD 20771, USA

<sup>e</sup>Astronomical Institute, Tohoku University, 6-3 Aramaki-zaaoba, Aoba-ku, Sendai, Miyagi 980-8578, Japan

<sup>f</sup>Department of Physics, Kyoto University, Kitashirakawa Oiwake-cho, Sakyo-ku, Kyoto, Kyoto 606-8502, Japan

<sup>g</sup>Department of Physics, Faculty of Science, Tokyo University of Science, Kagurazaka, Shinjuku-ku, Tokyo 162-0815, Japan

<sup>h</sup>Faculty of Science and Engineering, Chuo University, 1-13-27 Kasuga, Bunkyo, Tokyo 112-8551, Japan

<sup>i</sup>Department of Physics, University of Tokyo, 7-3-1 Hongo, Bunkyo, Tokyo 113-0033, Japan

<sup>j</sup>Department of Physics, Kindai University, 3-4-1 Kowakae, Higashi-Osaka, Osaka 577-8502, Japan

<sup>k</sup>Department of Physics, Konan University, 8-9-1 Okamoto, Higashinada, Kobe, Hyogo 658-8501

<sup>l</sup>Faculty of Informatics, Tohoku Gakuin University, 3-1 Shimizukoji, Wakabayashi-ku, Sendai, Miyagi 984-8588

<sup>m</sup>Science Education, Faculty of Education, Shizuoka University, Suruga-ku, Shizuoka, Shizuoka 422-8529, Japan

<sup>n</sup>Faculty of Education, Nara University of Education, Nara, Nara 630-8528, Japan

<sup>o</sup>Department of Earth and Space Science, Osaka University, 1-1 Machikaneyama-cho, Toyonaka, Osaka 560-0043, Japan

<sup>p</sup>Forefront Research Center, Osaka University, 1-1 Machikaneyama-cho, Toyonaka, Osaka 560-0043, Japan

<sup>q</sup>Department of Physics, Faculty of Science and Technology, Tokyo University of Science, 2641 Yamazaki, Noda, Chiba 270-8510, Japan

<sup>r</sup>Department of Physics, Nagoya University, Chikusa-ku, Nagoya, Aichi 464-8602, Japan

<sup>s</sup>Center for Space Science and Technology, University of Maryland, Baltimore County (UMBC), Baltimore, MD 21250, USA

<sup>t</sup>Department of Physics, School of Science and Technology, Meiji University, 1-1-1 Higashi Mita, Tama-ku, Kawasaki, Kanagawa 214-8571, Japan

<sup>u</sup>Japan Aerospace Exploration Agency, Institute of Space and Astronautical Science, 2-1-1, Sengen, Tsukuba, Ibaraki 305-8505, Japan

<sup>v</sup>Department of Physics, Kwansei Gakuin University, 2-2 Gakuen, Sanda, Hyogo 669-1337, Japan

<sup>w</sup>Department of Space and Astronautical Science, School of Physical Sciences, SOKENDAI (The Graduate University for Advanced Studies), 3-1-1 Yoshino-dai, Chuou-Ku, Sagamihara, Kanagawa 252-5210, Japan

<sup>x</sup>Advanced Technology Center, National Astronomical Observatory of Japan, 2-21-1 Osawa, Mitaka, Tokyo 181-8588, Japan

## ABSTRACT

Xtend is one of the two telescopes onboard the X-ray imaging and spectroscopy mission (XRISM), which was launched on September 7th, 2023. Xtend comprises the Soft X-ray Imager (SXI), an X-ray CCD camera, and the X-ray Mirror Assembly (XMA), a thin-foil-nested conically approximated Wolter-I optics. A large field of view of  $38' \times 38'$  over the energy range from 0.4 to 13 keV is realized by the combination of the SXI and XMA with a focal length of 5.6 m. The SXI employs four P-channel, back-illuminated type CCDs with a thick depletion layer of 200  $\mu\text{m}$ . The four CCD chips are arranged in a  $2 \times 2$  grid and cooled down to  $-110^\circ\text{C}$  with a single-stage Stirling cooler. Before the launch of XRISM, we conducted a month-long spacecraft thermal vacuum test. The performance verification of the SXI was successfully carried out in a course of multiple thermal cycles of the spacecraft. About a month after the launch of XRISM, the SXI was carefully activated and the soundness of its functionality was checked by a step-by-step process. Commissioning observations followed the initial operation. We here present pre- and post-launch results verifying the Xtend performance. All the in-orbit performances are consistent with those measured on ground and satisfy the mission requirement. Extensive calibration studies are ongoing.

**Keywords:** XRISM, Xtend, SXI, XMA, X-ray CCD, Back-illumination type CCD

## 1. INTRODUCTION

X-Ray Imaging and Spectroscopy Mission (XRISM) was successfully launched on September 7th, 2023 as the Japan’s seventh X-ray astronomical observatory.<sup>1</sup> The prime objectives of XRISM are to reveal material circulation and energy transfer in cosmic plasmas and to elucidate cosmic structures and objects.<sup>2</sup> XRISM pursues these objectives by means of the high-resolution X-ray spectroscopy with imaging, which is realized by two soft X-ray telescopes. One is a soft X-ray “spectroscopy” telescope, named Resolve,<sup>3</sup> and the other is a soft X-ray “imaging” telescope, named Xtend.<sup>4</sup> Both of them comprise an X-ray Mirror Assembly (XMA), a thin-foil-nested conically approximated Wolter-I optics, and a focal-plane detector with the same focal length of 5.6 m. The two XMAs share the same design and show almost the same imaging performance.<sup>5,6</sup> Resolve is

---

Further author information: (Send correspondence to K.M.)

K.M.: E-mail: mori@astro.miyazaki-u.ac.jp, Telephone: 81 985 58 7371

equipped with an X-ray micro-calorimeter array, a non-dispersive instrument achieving unprecedented, 7 eV (or better) energy resolution, and provides us with the high-resolution X-ray spectroscopy for diffuse sources as well as point sources.<sup>7,8</sup> Xtend is equipped with an X-ray CCD camera, named Soft X-ray Imager (SXI) and realizing a large field of view (FoV) of  $38' \times 38'$ , and provides us with the wide-field X-ray imaging spectroscopy. Resolve and Xtend point toward the same direction and the Xtend's FoV entirely covers the Resolve's limited FoV of  $3' \times 3'$ . The Xtend's pixel scale of  $1''.77$  is finer than the Resolve's pixel scale of  $30''$  and fully over-samples the point spread function (PSF), whose half power diameter (HPD) is about  $1'.3$ .<sup>5,6</sup> With these advanced imaging capabilities, Xtend monitors possible flux contamination to Resolve spectra from time-variable bright sources located outside the Resolve FoV, estimates local diffuse background from Galactic diffuse X-ray emission and/or solar wind charge exchange emission, and decomposes spatial structures within the Resolve's FoV. On the other hand, the Resolve's high-resolution spectrum gives definitive information to the interpretation of the Xtend's wide-field imaging spectroscopy. In one word, Xtend extends the Resolve's potential to the maximum and Resolve resolves the Xtend's spectrum into unprecedented details.

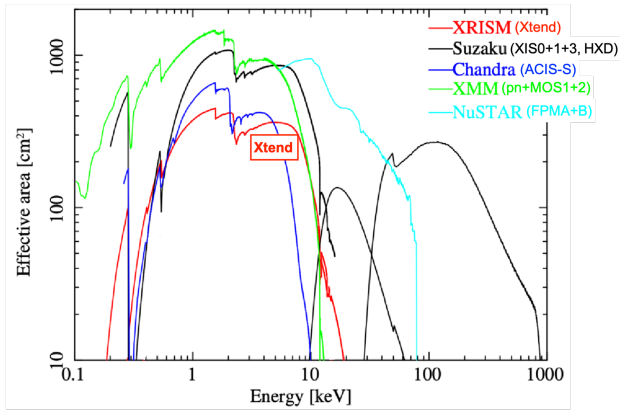


Figure 1. On-axis effective area of Xtend (red). Those of Suzaku (XIS0+XIS1+XIS3 and HXD; black), Chandra (ACIS-S; blue), XMM-Newton (pn+MOS1+MOS2; green), and NuSTAR (FPMA+FPMB; cyan) are also shown for comparison.

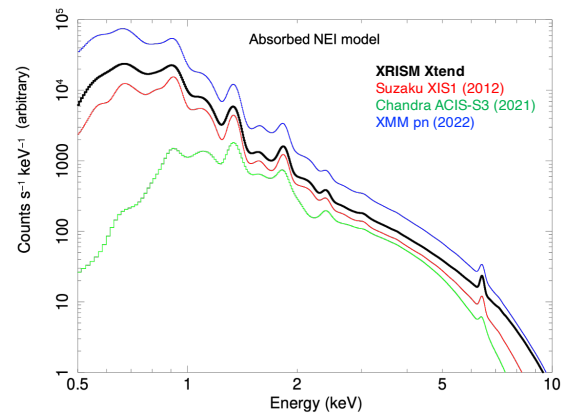


Figure 2. A simulated spectrum with an absorbed NEI model of Hitomi SXI, which is comparable to Xtend (black). Those of Suzaku XIS1 (as of 2012; red), Chandra ACIS-S3 (as of 2021; green), and XMM-Newton PN (as of 2022; blue) are also shown for comparison.

In comparison with the focal-plane CCD cameras flown in orbit so far, Xtend is characterized with several key features. The first one is a superior X-ray response in the high-energy band, especially in the 5-10 keV band in which X-ray emission lines from Fe-group elements can be observed. Fig. 1 and 2 show Xtend's on-axis effective area and simulated spectrum with an absorbed NEI model, respectively. The SXI employs P-channel back-illuminated type CCDs with a depletion layer thickness of  $200\ \mu\text{m}$ ,<sup>9-11</sup> following the *Hitomi* CCD camera.<sup>12</sup> Thanks to SXI's high quantum efficiency and XMA's large collecting area, Xtend has a large effective area in the high-energy band. A Gaussian-like simple energy response of the SXI CCD<sup>13</sup> in this band is also advantageous to reduce systematic uncertainties in the response function. This superior X-ray response in the high-energy band is useful for spatially-resolved spectroscopy of diffuse X-ray sources showing X-ray line emissions from Fe-group elements like young supernova remnants. The second one is its low, stable, and clean non-X-ray background (NXB), especially in the high energy band.<sup>14</sup> It is noteworthy that the background spectrum contains no strong lines overlapping major lines from astronomical sources. These properties of the Xtend background are mainly due to the fact that XRISM flies in a low earth orbit, whose radiation environment is relatively low and stable, and the material design of the CCD and detectors. This low, stable, and clean background is useful for detection of faint diffuse X-ray emissions like those from outskirts of galaxy clusters. The third one is the largest grasp at 7 keV among the focal-plane CCD cameras.<sup>15</sup> Grasp is defined as the product of effective area multiplied by effective FoV, and considered as a figure of merit to capture

diffuse X-ray emission. This feature is useful for studies of hard X-ray diffuse sources and also transient diffuse emission like solar wind charge exchange emission. The forth one is its large FoV, allowing serendipitous source detection in the surrounding area of target sources. Utilizing this feature, the Xtend Transient Search program is in operation, in which a transient source search is performed for down-linked Xtend data once a day.<sup>16</sup> All these key features, combined with a long-exposure nature of XRISM observations, will derive new results even from Xtend data alone.

Before the launch of XRISM, we conducted a month-long spacecraft thermal vacuum test. The performance verification of the SXI was successfully carried out in a course of multiple thermal cycles of the spacecraft. About a month after the launch of XRISM, the SXI was carefully activated and the soundness of its functionality was checked by a step-by-step process. In this paper, we report the pre- and post-launch status of Xtend, mostly focusing on the SXI. The calibration studies of the XMA are presented elsewhere.<sup>5,6,17</sup> The details of the SXI initial operation are presented separately in Ref. 18. CCD spectra shown below are all made with grade 0, 2, 3, 4, and 6 events unless otherwise indicated.

## 2. SPECIFICATIONS AND OBSERVATION MODES

Table 1. Specifications of Xtend

Field of view	$38' \times 38'$
Format	$640 \times 640$ logical pixels per 1CCD
Pixel scale	$1''.77 \times 1''.77$
Energy range	0.4–13 keV
Energy resolution	$\sim 180$ eV (FWHM) at 5.9 keV
Effective area <sup>†</sup>	$\sim 430$ cm <sup>2</sup> at 1.5 keV $\sim 350$ cm <sup>2</sup> at 6 keV
Frame cycle	4 seconds
Charge injection	every 80 logical rows

<sup>†</sup> to be updated by in-orbit calibration

Xtend’s SXI and XMA have basically identical designs to the *Hitomi* X-ray CCD camera<sup>12</sup> and X-ray mirror,<sup>19</sup> respectively. The changes taken in Xtend are described in Ref.4,13,20. Table 1 summarizes specifications of Xtend. The SXI has four CCDs, arranged in a 2×2 grid, to achieve a large FoV of  $38' \times 38'$ . One CCD has a  $1280 \times 1280$  *physical* pixel format, which becomes a  $640 \times 640$  *logical* pixel format through on-chip 2×2 binning. The logical pixel size is  $48 \mu\text{m} \times 48 \mu\text{m}$ , which corresponds to  $1''.77 \times 1''.77$ . The energy range is defined as 0.4–13 keV and well overlaps with that of Resolve. The energy resolution is  $\sim 180$  eV (FWHM) at 5.9 keV, which is the average value of 4 CCDs and the individual values are shown in Section 4. The effective area values in the table are derived from ground calibrations and will be updated by ongoing in-orbit calibrations. The frame cycle is 4 seconds, during which two halves of the imaging area, called segments, are separately and simultaneously read out. We apply the charge injection (CI) technique to mitigate the charge loss due to transfer inefficiency<sup>21–23</sup> and a CI row is placed every 80 logical rows.

Table 2. Observation modes of Xtend

Mode	Fraction of read-out area over imaging area	Exposure time (sec)	Number of exposure per frame	Live time fraction <sup>†</sup>
Full window	1	3.96	1	0.99
1/8 window	1/8	0.46	8	0.93
1/8 window + burst	1/8	0.06	8	0.12
Full window + burst	1	0.06	1	0.015

<sup>†</sup> excluding charge transfer time, during which photons detected are recognized as trailing events

Tab. 2 lists observation modes of Xtend. The full window mode is a standard observation mode. The entire imaging area is read out per frame cycle. The charge transfer time accounts for just about 1% of the frame cycle and the live time fraction (LTF) is about 99%. The 1/8 window mode reads out only 1/8 of the entire imaging area around on-axis position and repeats the exposure eight times per frame cycle. Since the exposure time is reduced by a factor of 8, the pile-up tolerance is increased by the same amount. The 1/8 window + burst mode reads out the same area as the 1/8 window mode but reduces the exposure time down to 0.06 sec. The pile-up tolerance is further increased in this mode in compensation for the loss of LTF; the exposure time (0.06 sec) is much shorter than the read-out time for the 1/8 area (0.5 sec). The full window + burst mode is made for calibration purpose and not open for guest observers. In this mode, the exposure time is significantly shorter the read-out time for the entire imaging area so that the LTF is extremely low.

In terms of the observation mode, CCD1 and CCD2 are one pair, and CCD3 and CCD4 are the other pair. Two CCDs in the same pair operate in the same observation mode, and the two pairs can operate in different observation mode. The observation axis of Xtend is located in CCD2, and the observation mode for the pair of CCD1 and CCD2 can be selected by observers according to their observation purposes whereas that for the pair of CCD3 and CCD4 is always the full window mode.

As is shown above, event pile-up is always a concern for CCD detectors. Therefore, we developed the pile-up simulator dedicated for Xtend, which is presented in Ref. 24.

In our ground experiments, we developed a new observation mode, which is not listed in Tab. 2. The new observation mode is a countermeasure against an issue we encountered in sub-system level tests in ground. We did not observe the issue in the system-level tests in ground nor in orbit. We do not expect to use the new observation mode in future for Xtend. The details of the issue and the new observation mode are presented in Ref. 25.

### 3. PERFORMANCE VERIFICATION IN SPACECRAFT THERMAL VACUUM TEST

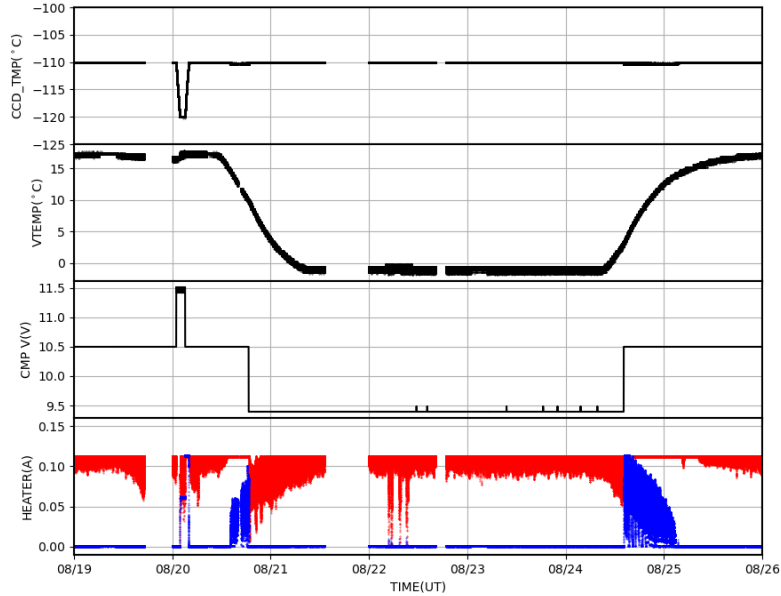


Figure 3. Time histories of CCD temperature (top), video temperature (second from the top), cooler compressor voltage (third from the top), and heater currents (bottom). Two heaters are attached to the plate on which CCDs are installed. Red and blue colors in the bottom plot indicates the two different heater currents.

After a series of performance verification tests in sub-system level, including the thermal vacuum, vibration, and acoustic tests,<sup>13</sup> the SXI sub-system was installed to the XRISM spacecraft in April 2022. The spacecraft system level tests, including initial electrical, thermal vacuum, mechanical environmental, and final electrical tests, started in May 2022 and ended in March 2023.<sup>1</sup> Among these tests, the spacecraft thermal vacuum test was the only occasion for us to cool the CCDs and verify the performances of the SXI sub-system in detail.

The spacecraft thermal vacuum test was performed over a period of a month in August 2022, during which the spacecraft experienced multiple thermal cycles. Fig. 3 shows a time history of the CCD temperature for a given week along with those of the video temperature, cooler compressor voltage, and heater currents. Here, the video temperature is a kind of proxy of the thermal cycle phase; in this period, the thermal cycle phase first shifted from the hot side to the cold side and then shifted again from the cold side to the hot side. Through the swings in the thermal environment, Xtend kept its CCD temperature constant at  $-110\text{ }^{\circ}\text{C}$ , which is the initial operating temperature in orbit. The cooler compressor voltage was adjusted so that the total duty cycle of the two heaters, attached to the plate on which CCDs are installed, was around 50%. It was also verified that Xtend can cool the CCD down to  $-120\text{ }^{\circ}\text{C}$  in this period.

In this test, the spectroscopic performance was also verified by evaluating spectra of X-ray events from the  $^{55}\text{Fe}$  calibration sources. In addition, adjustment of the charge injection amount, confirmation of optical blocking power, and mock run of nominal operation were also performed without major problems.

#### 4. PERFORMANCES IN ORBIT

Following the critical operation of the spacecraft, commissioning operation of the bus components, and start-up operation of Resolve after the launch of XRISM, we conducted the start-up operation of Xtend spending 5 days from October 17th, 2023. This start-up operation went well as we tested on ground. All the subsequent commissioning operations were also successfully performed. Here we summarize initial results verifying the Xtend performance.

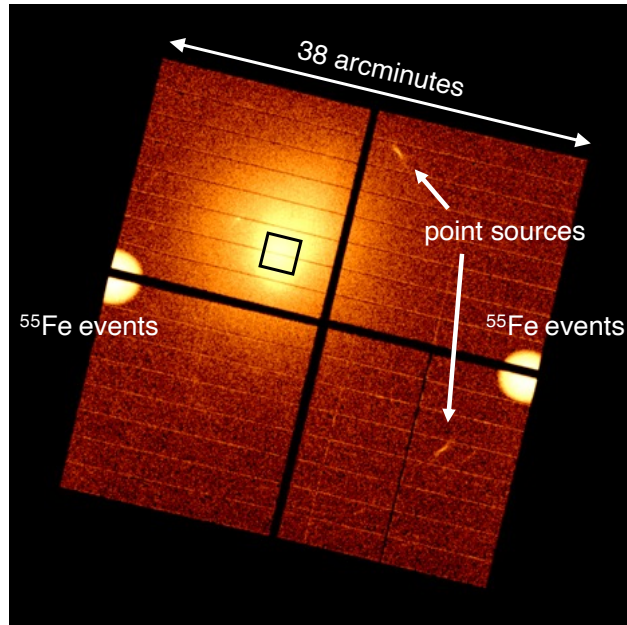


Figure 4. The first light image of Xtend. The galaxy cluster Abell 2319 and some off-axis point sources are captured. X-ray events from the  $^{55}\text{Fe}$  calibration sources are seen at the corners of CCDs. The black box indicates the FoV of Resolve.

Fig. 4 shows the first light image of Xtend. The galaxy cluster Abell 2319 is captured in this image. This is truly the first light image in the sense that XRISM was pointing to this galaxy cluster before and through the start-up operation of Xtend. This image was made from the same data as the public first light image



released by JAXA, but without Vignetting correction, energy selection, or, intentional color-scale adjustment so that this can be regarded as an unfiltered image. A grade selection was applied. The entire region covering the  $38' \times 38'$  FoV is fully functional for X-ray detection except for bad columns known from ground tests, which is seen as a dark lane running at the center of the CCD positioned at bottom right in this figure. Some off-axis point sources are also detected. Their arc-like shape is due to the skewed PSF of the XMA at off-axis. The CCDs are not aligned perfectly parallel so that the width of the gap between CCD active regions varies depending on the position from  $40''$  to  $60''$ . The corners of CCDs are irradiated with X-ray from the  $^{55}\text{Fe}$  calibration sources. The count rates are  $\sim 1 \text{ counts sec}^{-1} \text{ CCD}^{-1}$  as of October 2023. The Xtend FoV completely encompasses the Resolve FoV by shifting its geometrical center by  $\sim 5'$ . Please note that the positions of the CI rows were later shifted by 35 rows not to interfere with an on-axis source.<sup>18</sup> The spacing of the CI rows was not changed and remains at 80 rows.

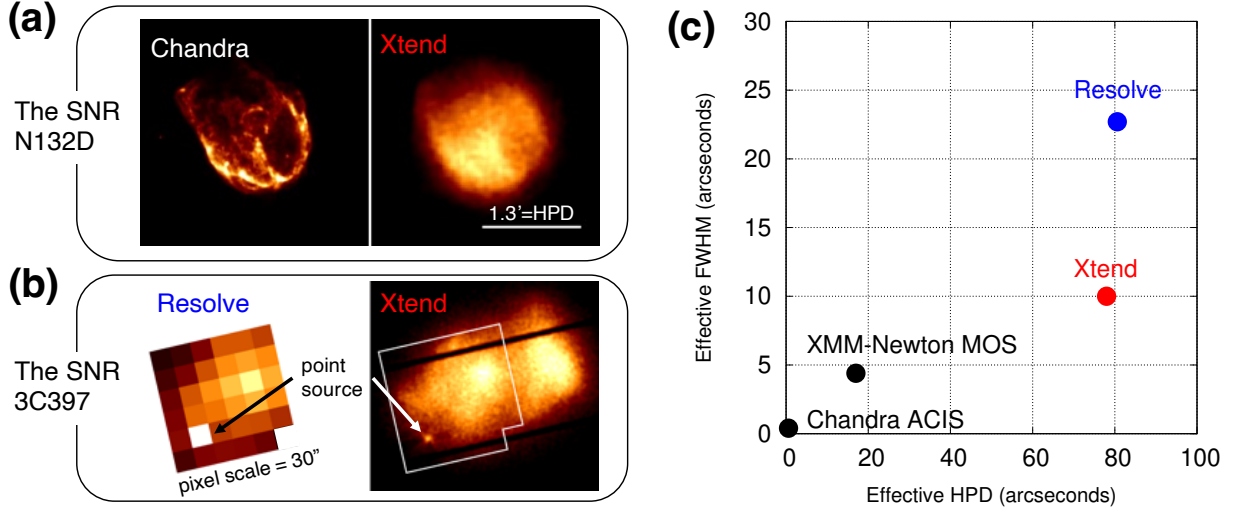


Figure 5. (a) Chandra and Xtend images of the supernova remnant N132D. The white bar indicates the size of  $1/3$ , which is the same as the HPD of the Xtend XMA.<sup>6</sup> (b) Resolve and Xtend images of the supernova remnant 3C397. The Resolve FoV excluding the calibration pixel are superimposed on the Xtend image with a white polygon. A known background point source is detected in both images. (c) Relationships between the FWHM and HPD of point-source images obtained with Xtend (red) and Resolve (blue) as well as Chandra ACIS and XMM-Newton MOS (black).

Fig. 5(a) shows Chandra and Xtend images of the supernova remnant N132D in the Large Magellanic Cloud. A three-color version of the Xtend image was public-released by JAXA. In spite of that the diameter of this remnant is almost the same as the HPD of the XMA of  $1/3$ , the internal structures, like central bar and southwestern void, can be identified even in the Xtend image. Fig. 5(b) shows Resolve and Xtend images of the supernova remnant 3C397 in our Galaxy. A known background point source is detected in both images. You can find that the position of the source can be more precisely identified in the Xtend image. These characteristics can be understood with Fig. 5(c), where relationships between the FWHM and HPD of point-source images obtained with Xtend and Resolve as well as Chandra ACIS and XMM-Newton MOS are plotted. Both the FWHM and HPD of a point-source image reflect not only the X-ray mirror performance but also the blurring due to pixel size of detectors, system attitude reconstruction inaccuracy, and so on. Although, in terms of the effective HPD, the value of Xtend is about five times larger than that of XMM-Newton, in terms of the effective FWHM, the value of Xtend is just twice larger than that of XMM-Newton. The Xtend's sharp PSF, FWHM of  $\sim 10''$ , is beneficial to resolve spatial structures and detect point sources. However, we need to keep it mind that the HPD is more important measure to evaluate photon leakage from and to neighboring regions. In the comparison between Resolve and Xtend, the difference in effective FWHM directly reflects the difference in pixel scale because the FWHM of the XMA's PSF is in between the pixel scales of Resolve and Xtend. In this regard, the effective HPDs of Resolve and Xtend are more or less the same.



Regarding XMA-related items, the HPD and effective area of Xtend were also measured to be consistent with results obtained in ground calibrations and satisfy mission requirements.<sup>6</sup>

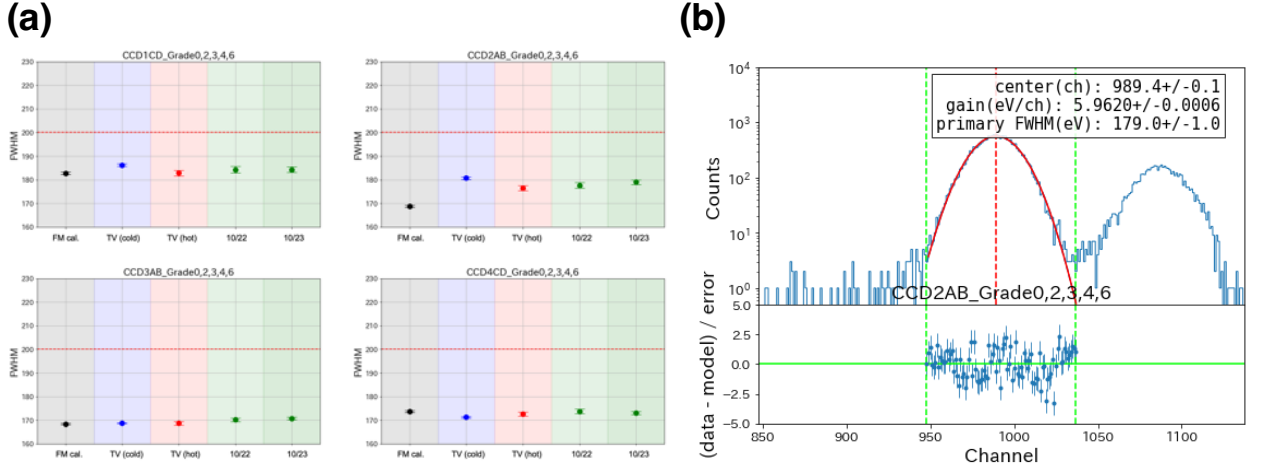


Figure 6. (a) Energy resolution measured in the calibration in the sub-system level test (black), the cold side (blue) and hot side (red) of spacecraft thermal vacuum test, and on October 22th (light green) and 23th (green), 2023 in orbit. Those of CCD1 (top left), CCD2 (top right), CCD3 (bottom left), and CCD4 (bottom right) are shown. The red dotted line indicates the requirement imposed on Xtend at the beginning of life of XRISM. (b) Spectrum of X-ray events from the <sup>55</sup>Fe calibration source taken with CCD2 (on-axis CCD). CTI corrections with parameters determined on ground are applied. The red curve is the best-fit single Gaussian to the Mn-K $\alpha$  line.

Fig. 6 summarizes energy resolution measured on ground and in orbit. The Mn-K $\alpha$  line in the spectrum of X-ray events from the <sup>55</sup>Fe calibration sources is fitted with a single Gaussian and the FWHM derived in the unit of eV are shown. CTI corrections with parameters determined on ground are applied in the data analysis.<sup>23</sup> A single Gaussian reasonably well fit the data with this level of statistics. The energy resolution measured in orbit was  $\sim 180$  eV and satisfied the mission requirement of 200 eV at the beginning of life. Results obtained in orbit are fully consistent with those obtained on ground. In the case of the *Hitomi* X-ray CCD camera, the energy resolution measured in orbit was degraded by  $\sim 10$  eV in comparison with that measured on ground.<sup>14</sup> Although the reason of the degradation was not clear, the *Hitomi* spectrum might have been partly affected by a light leak issue, which we took multiple measures in XRISM/Xtend.<sup>4,26</sup>

Fig. 7 shows the Xtend spectrum of the quasar 3C 273. This bright quasar spectrum clearly demonstrates that Xtend covers the energy range of 0.4–13 keV. Actually, as you can see, Xtend is still sensitive to X-ray photons beyond this energy band. We define this official energy band for which extensive calibration work is performed. Calibration uncertainties in the linearity of energy scale and the tail component of response function might be a concern above 13 keV and below 0.4 keV, respectively.

Fig. 8 shows the NXB spectra of Xtend and the *Hitomi* X-ray CCD camera. There is no major difference between the two spectra. This is as expected because the orbit of the satellite and the design of the camera are the same. Prominent lines are labeled in this figure. In addition, you can find an apparent broad line at  $\sim 8.3$  keV and a weak line at  $\sim 13.4$  keV. The former is likely a blend of Ni K $\beta$  and Au L $\alpha$ , and the latter is likely a Au L $\gamma$  blend. As stated above, in this spectrum, there is no strong lines overlapping major lines from astronomical sources. This cleanness along with its low and stable flux make it easy to model the NXB spectrum of Xtend and ensure its reproducibility.

Lastly, we mention that there is no apparent contamination build-up as experienced by the Suzaku CCD cameras<sup>27</sup> as of writing this paper, more than half a year passed after the launch. We will continue to monitor this issue.

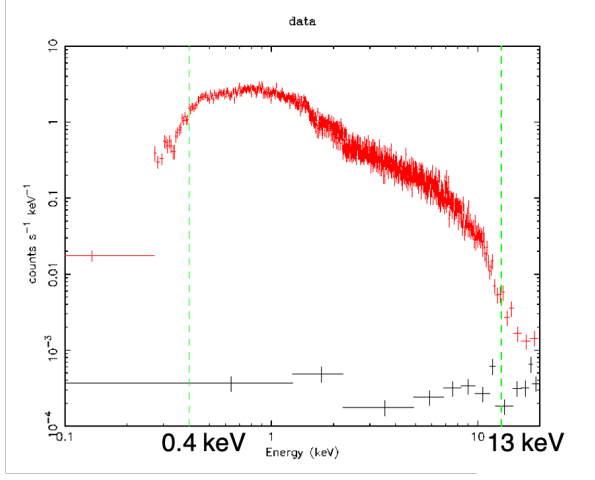


Figure 7. Xtend spectrum of the quasar 3C 273 (red) and its normalized NXB spectrum (black). The two vertical green dashed lines indicate the boundaries of Xtend’s official energy range of 0.4–13 keV.

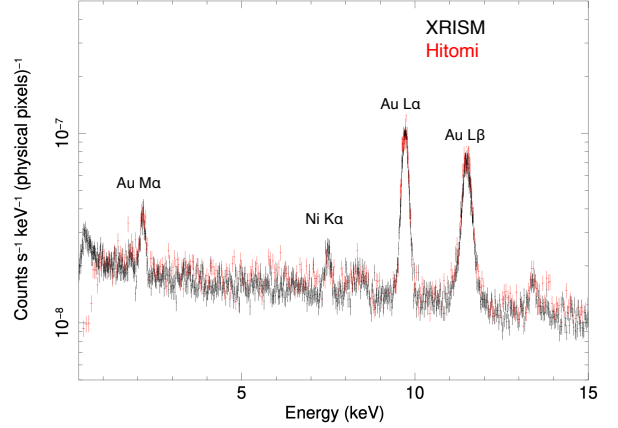


Figure 8. Non-X-ray background spectra of Xtend (black) and the *Hitomi* X-ray CCD camera (red).

## 5. SUMMARY

Xtend is a soft X-ray imaging telescope developed for XRISM, consisting of the Soft X-ray Imager (SXI), an X-ray CCD camera, and the X-ray Mirror Assembly (XMA), a thin-foil-nested conically approximated Wolter-I optics. Combining the SXI and XMA with a focal length of 5.6 m, a field of view  $38' \times 38'$  of over the energy range from 0.4 to 13 keV is realized. Xtend was successfully started up 40 days after the launch of the satellite and all the commissioning operations were also successfully performed. All the performances, including FoV, HPD,<sup>6</sup> effective area,<sup>6</sup> energy resolution, non-X-ray background, and contamination, are fully consistent with those measured in ground tests and satisfy mission requirements. Now we are ready for science outputs. Calibration activities are on-going.

## ACKNOWLEDGMENTS

We acknowledge all the supports from Hamamatsu Photonics K.K., Mitsubishi Heavy Industries Ltd., and Sumitomo Heavy Industries Ltd. to develop CCD, SXI system, and cooler component, respectively, including those in the ASTRO-H era. This work was supported by JSPS KAKENHI Grant Numbers 19K21884, 20H01947, 20KK0071, 23K20239, 21J00031, 22KJ3059, 24K17093, 21K20372, 23K22540, 22H01269, 21H04493, 24K17105, 21K03615, 24K00677, 21K13963, 23K22536, 21H01095, 23K20850, 23H00128, 20H00175, 20KK0071, 24H00253.

## REFERENCES

- [1] Tashiro, M. et al., “Development and Operation Status of X-Ray Imaging and Spectroscopy Mission (XRISM),” *Proc. SPIE*, in press (2024).
- [2] Tashiro, M. et al., “Status of x-ray imaging and spectroscopy mission (XRISM),” *Proc. SPIE* **11444**, 1144422 (Dec. 2020).
- [3] Ishisaki, Y. et al., “Resolve Instrument on X-ray Astronomy Recovery Mission (XARM),” *Journal of Low Temperature Physics* **193**, 991–995 (Dec. 2018).
- [4] Hayashida, K. et al., “Soft x-ray imaging telescope (Xtend) onboard X-ray Astronomy Recovery Mission (XARM),” *Proc. SPIE* **10699**, 1069923 (July 2018).
- [5] Hayashi, T. et al., “In-orbit performance of the XMA for XRISM/Resolve,” *Proc. SPIE*, in press (2024).

- [6] Tamura, K. et al., “In-orbit performance of the Xtend-XMA onboard XRISM,” Proc. SPIE, in press (2024).
- [7] Kelly, R. et al., “Overview and inflight performance of the resolve high-resolution soft X-Ray spectrometer on the X-Ray imaging and spectroscopy mission,” Proc. SPIE, in press (2024).
- [8] Porter, F. et al., “In-flight performance of the XRISM/Resolve detector system,” Proc. SPIE, in press (2024).
- [9] Ozawa, H. et al., “Development of p-type CCD for the NeXT: the next Japanese x-ray astronomical satellite mission,” Proc. SPIE **6266**, 62662N (June 2006).
- [10] Takagi, S. et al., “Development of fully depleted and back-illuminated charge-coupled devices for soft x-ray imager onboard the NeXT satellite,” Proc. SPIE **6266**, 62663V (June 2006).
- [11] Ueda, S. et al., “Development of the x-ray CCD for SXI on board ASTRO-H,” Proc. SPIE **8145**, 814504 (Sept. 2011).
- [12] Tanaka, T. et al., “Soft X-ray Imager aboard Hitomi (ASTRO-H),” *Journal of Astronomical Telescopes, Instruments, and Systems* **4**, 011211 (Jan. 2018).
- [13] Mori, K. et al., “Xtend, the soft x-ray imaging telescope for the X-Ray Imaging and Spectroscopy Mission (XRISM),” Proc. SPIE **12181**, 121811T (Aug. 2022).
- [14] Nakajima, H. et al., “In-orbit performance of the soft X-ray imaging system aboard Hitomi (ASTRO-H),” PASJ **70**, 21 (Mar. 2018).
- [15] Nakajima, H. and Hitomi Collaboration, “Astronomical imaging with the X-ray observatory Hitomi,” *Nuclear Instruments and Methods in Physics Research A* **873**, 16–20 (Nov. 2017).
- [16] Tsuboi, Y. et al., “X-ray transient search using XRISM/Xtend,” Proc. SPIE, in press (2024).
- [17] Boissay-Malaquin, R. et al., “X-ray Mirror Assembly for the X-Ray Imaging and Spectroscopy Mission (XRISM): comparison between ground calibration measurements and raytracing simulations,” Proc. SPIE, in press (2024).
- [18] Suzuki, H. et al., “Initial operations of the Soft X-ray Imager onboard XRISM,” Proc. SPIE, in press (2024).
- [19] Iizuka, R. et al., “Ground-based x-ray calibration of the Astro-H/Hitomi soft x-ray telescopes,” *Journal of Astronomical Telescopes, Instruments, and Systems* **4**, 011213 (Jan. 2018).
- [20] Nakajima, H. et al., “Soft x-ray imager (SXI) for Xtend onboard X-Ray Imaging and Spectroscopy Mission (XRISM),” Proc. SPIE **11444**, 1144423 (Dec. 2020).
- [21] Uchiyama, H. et al., “New CTI Correction Method for Spaced-Row Charge Injection of the Suzaku X-Ray Imaging Spectrometer,” PASJ **61**, S9–S15 (Jan. 2009).
- [22] Nobukawa, K. K. et al., “Use of a charge-injection technique to improve performance of the Soft X-ray Imager aboard ASTRO-H,” *Nuclear Instruments and Methods in Physics Research A* **765**, 269–274 (Nov. 2014).
- [23] Kanemaru, Y. et al., “Experimental studies on the charge transfer inefficiency of ccd developed for the soft x-ray imaging telescope xtend aboard the xrism satellite,” *Nuclear Instruments and Methods in Physics Research A* **984**, 164646 (2020).
- [24] Yoneyama, T. et al., “Pile-up simulator for XRISM/Xtend,” Proc. SPIE, in press (2024).
- [25] Noda, H. et al., “New CCD driving technique to suppress anomalous charge intrusion from outside the imaging area for soft X-ray imager of Xtend onboard XRISM,” Proc. SPIE, in press (2024).
- [26] Uchida, H. et al., “Optical blocking performance of ccds developed for the x-ray astronomy satellite xrism,” *Nuclear Instruments and Methods in Physics Research A* **978**, 164374 (2020).
- [27] [https://darts.isas.jaxa.jp/astro/suzaku/analysis/doc/suzaku\\_td/](https://darts.isas.jaxa.jp/astro/suzaku/analysis/doc/suzaku_td/)